A Serendipitous Discovery of GeV Gamma-Ray Emission from Supernova 2004dj in a Survey of Nearby Star-forming Galaxies with Fermi-LAT

Shao-Qiang Xi[1,2], Ruo-Yu Liu[1,2] , Xiang-Yu Wang[1,2] , Rui-Zhi Yang[3,4], Qiang Yuan[5], and Bing Zhang[6]

[1] School of Astronomy and Space Science, Nanjing University, Nanjing 210023, People's Republic of China; ryliu@nju.edu.cn, xywang@nju.edu.cn
[2] Key laboratory of Modern Astronomy and Astrophysics (Nanjing University), Ministry of Education, Nanjing 210023, People's Republic of China
[3] Key Laboratory for Research in Galaxies and Cosmology, Department of Astronomy, University of Science and Technology of China, Hefei, Anhui 230026, People's Republic of China
[4] School of Astronomy and Space Science, University of Science and Technology of China, Hefei, Anhui 230026, People's Republic of China
[5] Key Laboratory of Dark Matter and Space Astronomy, Purple Mountain Observatory, Chinese Academy of Sciences, Nanjing 210033, People's Republic of China
[6] Department of Physics and Astronomy, University of Nevada, Las Vegas, 4505 Maryland Parkway, Las Vegas, NV 89154-4002, USA

Abstract

The interaction between a supernova ejecta and the circumstellar medium drives a strong shock wave that accelerates particles (i.e., electrons and protons). The radio and X-ray emission observed after the supernova explosion can be interpreted as synchrotron emission from accelerated electrons. The accelerated protons are expected to produce GeV–TeV gamma-ray emission via proton–proton collisions, but the flux is usually low since only a small fraction of the supernova kinetic energy is converted into the shock energy at the very early time. The low gamma-ray flux of the nearest supernova explosion, SN 1987A, agrees with this picture. Here we report a serendipitous discovery of a fading GeV gamma-ray source in spatial coincidence with one of the nearest and brightest supernova—SN 2004dj from our gamma-ray survey of nearby star-forming galaxies with Fermi-LAT. The total gamma-ray energy released by SN 2004dj is about 6×10^{47} erg. We interpret this gamma-ray emission arising from the supernova ejecta interacting with a surrounding high-density shell, which decelerates the ejecta and converts $\sim$1% of the SN kinetic energy to relativistic protons.

Unified Astronomy Thesaurus concepts: Gamma-ray sources (633); Type II supernovae (1731); Non-thermal radiation sources (1119)

1. Introduction

As the supernova (SN) ejecta expands in the circumstellar medium, a collisionless shock forms. The collisionless shock accelerates electrons to high energies, which emit photons from the radio–submillimeter through X-ray energies, as have been observed from a large number of supernovae. Protons may also be accelerated by the shocks and they can produce GeV–TeV gamma-rays via the neutral pion decay (Berezhko et al. 2011, 2015; Murase et al. 2011; Li 2019; Wang et al. 2019). Gamma-rays can also be produced by nonthermal bremsstrahlung and inverse Compton radiation. Indeed, gamma-ray emission from GeV to TeV energies have been detected from a dozen of historic supernova remnants (SNRs) in our Galaxy. Although SNRs are distinct from the early supernova as they have already swept up a large amount of circumstellar medium (CSM), the physics governing the production of gamma-rays is the same. Thus, gamma-ray emission from supernovae, particularly from the nearest supernova SN 1987A, has been predicted for a long while (Berezhko et al. 2011, 2015). Recently, Malyshev et al. (2019) reported a recent enhancement of the GeV emission from the SN 1987A region as observed with Fermi-LAT. But the location of this source overlaps with several other potential gamma-ray sources, so the nature of the GeV emission remains to be clarified.

Gamma-ray emission from SNe IIn and from superluminous SNe have been searched by Ackermann et al. (2015) and Renault-Tinacci et al. (2018), respectively. No evidence for a signal was found, but their observational limits start to reach interesting parameter ranges expected by the theory. Recently, Yuan et al. (2018) reported the detection of a variable gamma-ray source spatially and temporally consistent with a peculiar

supernova, iPTF14hls. However, there is a quasar in the error circle of the Fermi-LAT source, which is a blazar candidate according to the infrared data. The lack of multiwavelength observations of this quasar makes it difficult to conclusively address its connection with the gamma-ray variable source.

SN 2004dj is the nearest and brightest SN IIP exploded on about 2004 July 28 (UT) in the galaxy NGC 2403 at a distance of about 3.5 Mpc (Nakano et al. 2004; Patat et al. 2004; Vinkó et al. 2006; Nayana et al. 2018). The progenitors of SNe IIP are thought to be red supergiants. The fast moving stellar ejecta interacts with the CSM created by the stellar wind of the red supergiants. SN 2004dj was detected in a wide range of wavelengths from radio through infrared to X-rays during the first several years after the explosion (Meikle et al. 2011; Chakraborti et al. 2012; Nayana et al. 2018).

In this Letter, we report a serendipitous discovery of a GeV gamma-ray source whose position is compatible within uncertainties with the position of SN 2004dj. This discovery is made when we search for GeV emission from nearby star-forming galaxies. By analyzing the 11.4 yr of Fermi-LAT data, we find a GeV source from the direction of the nearby galaxy NGC 2403. The flux of the this source, however, does not obey the well-known relation between the gamma-ray luminosity and infrared luminosity for star-forming galaxies (Ackermann et al. 2012), disfavoring the usual cosmic ray–interstellar medium (ISM) interaction origin. We also find the flux is decaying during the Fermi-LAT observation period from 2008 to the present. Motivated by this, we search for transient sources in the error region of the gamma-ray emission and find that SN 2004dj lies within the error region.

2. Sample Selection and Data Analysis

We perform a search for possible gamma-ray emission from galaxies in the IRAS Revised Bright Galaxies Sample (Sanders et al. 2003), using 11.4 yr of gamma-ray data taken by the Fermi-LAT telescope (Atwood et al. 2009). This is a complete flux-limited sample of all extragalactic objects brighter than 5.24 Jy at 60 μm, covering the entire sky surveyed by IRAS at Galactic latitudes $|b| > 5°$. In the sample, 15 infrared (IR)-bright galaxies have been detected in gamma-rays with Fermi-LAT and listed in Fermi-LAT Fourth Source Catalog (4FGL; Abdollahi et al. 2020), including six galaxies with AGNs (i.e., Cen A, IC 4402, NGC 3067, NGC 3683, NGC 1275, NGC 3424; Peng et al. 2019), seven star-forming galaxies (SMC, LMC, M31, NGC 253, M82, NGC 2146, Arp 220; Abdo et al. 2010a; Ackermann et al. 2012; Tang et al. 2014; Griffin et al. 2016; Peng et al. 2016), and two star-forming galaxies with obscured AGNs (NGC 1068, NGC 4945; Ackermann et al. 2012). These galaxies are excluded, leading to a sample of 614 galaxies.

This work uses ~11.4 yr (MET 239557417-595385929) of Fermi-LAT Pass8 SOURCE class events with reconstructed energies between 300 MeV and 500 GeV, excluding those with a zenith angle larger than 90° to avoid Earth limb contamination. We implement a standard sequence of analysis steps. For each IR-bright galaxy, we select the events in a $17° × 17°$ region of interest (ROI) centered at the galactic center and use the *gtmktime* tool to select time intervals expressed by (DATA_QUAL > 0) && (LAT_CONFIG==1). We bin the data in 20 logarithmically spaced bins in energy and in a spatial bin of 0°025 per pixel. We make use of recent developments of the Science Tools for likelihood analysis. The background model for each celestial ROI contains all sources listed in the 4FGL along with the standard diffuse emission background, i.e., the foreground for Galactic diffuse emission (gll_iem_v7.fits) released and described by the Fermi-LAT collaboration through the Fermi Science Support Center (Acero et al. 2016) and the background for the spatially isotropic diffuse emission with a spectral shape described by iso_P8R3_SOURCE_V2_v01.txt. We ignore the energy dispersion, which is not important for the analysis above 300 MeV. We employ the *gttsmap* tool to evaluate the $6° × 6°$ map of the test statistic (TS), defined as TS $= -2(\ln L_0 - \ln L)$, where L_0 is the maximum-likelihood value for null hypothesis and L is the maximum-likelihood with the additional point source with a power-law spectrum, and then survey the new gamma-ray sources when the significance of the gamma-ray excess above backgrounds is TS > 25. The best location and uncertainty of the new sources can be determined by maximizing the TS value and using the distribution of the localization test statistic (LTS), defined by twice the log of the likelihood ratio of any position with respect to the maximum. We claim a gamma-ray source associated with a target galaxy when the target galaxy lies within the 95% confidence location region of the gamma-ray source. Note that new background sources could be found and, if so, we redo the analysis using an updated background model including the new background sources. In the likelihood analysis, we allow all the sources that are separated from the ROI center by less than 6°5 to have a free normalization and fixed index.[7] The

normalizations of both Galactic and extragalactic diffuse emission models are left free.

3. Results

Our analysis results in the detection of two new gamma-ray sources that are, respectively, spatially coincident with the galaxy Arp 299 and the galaxy M33 (see Table 1; more details can be found in Xi et al. 2020). In addition, we find that the gamma-ray source reported in 4FGL (4FGL J0737.4+6535) is spatially coincident with the galaxy NGC 2403, since the best location of 4FGL J0737.4+6535 is within the optical disk (about 8 kpc in diameter) of NGC 2403. For the rest of the galaxies in our sample, we do not find any significant emission.

It has been found that there is an empirical correlation between the gamma-ray luminosity in (0.1–100) GeV and total IR luminosity (8–1000 μm) for Local Group galaxies and nearby star-forming galaxies (Ackermann et al. 2012; Peng et al. 2016). This correlation is generally interpreted as that the gamma-ray emission arises from cosmic-ray (CR) protons interacting with the ISM via the proton–proton (pp) collisions (Ackermann et al. 2012; Zhang et al. 2019). In Figure 1, we show the relation between the gamma-ray luminosity and IR luminosity for the three gamma-ray sources found in our work. While Arp 299 and M33 are well consistent with the aforementioned correlation, NGC 2403 is obviously an outlier. The latter is even above the theoretical calorimetric limit, which is obtained by considering that all of the cosmic-ray energy is converted into secondary particles and may be achieved only in those gas-rich starburst galaxies with luminous IR radiation (e.g., $L_{8-1000 \, \mu m} > 10^{11} L_\odot$). This suggests that the gamma-ray emission from NGC 2403 cannot primarily arise from the CR–ISM interaction in the galaxy.

We generate the light curves of the target gamma-ray source with eight and four time bins, respectively. In each time bin, all sources (including the target source) within 6°5 of the ROI center have spectra fixed to the shapes obtained from the full data set analysis, and only normalizations are allowed to vary. As shown in Figure 2, the fluxes appear to decay with time in both cases. We then use a likelihood-based statistic to test the significance of the variability. Following the definition in 2FGL (Nolan et al. 2012), the variability index from the likelihood analysis is constructed, with a value in the null hypothesis where the source flux is constant across the full time period, and the value under the alternate hypothesis where the flux in each bin is optimized: $\mathrm{TS_{var}} = \sum_{i=1}^{N} 2 × (\log(L_i(F_i)) - \log(L_i(F_{mean})))$, where L_i is the likelihood corresponding to bin i, F_i is the best-fit flux for bin i, and F_{mean} is the best-fit flux for the full period assuming a constant flux. The statistic $\mathrm{TS_{var}}$ is expected to be distributed, in the null case, as $\chi^2_{N-1}(\mathrm{TS_{var}})$. We find that the gamma-ray emission is variable at a confidence level of 3.3σ for the analysis with four time bins and of 2.7σ for the analysis with eight time bins, respectively. The variability can be also seen from Figure 3, which shows an obvious gamma-ray excess over the background using the first 5.7 yr of the Fermi-LAT observation, but no significant excess in the second 5.7 yr. In this case, the most significant variability is obtained at the 3.5σ ($\mathrm{TS_{var}} = 13.0$) significance level. We can estimate a post-trial significance level at 3.1σ considering the number of trials is three as we test the variability using two, four, and eight time bins respectively. Thus, we suggest that the gamma-ray source 4FGL J0737.4+6535 in the region of NGC 2403 is fading with time.

---

[7] If a gamma-ray source is spatially coincident with one of the target galaxies, we first free the spectral parameters (including the normalizations and the spectral indices) of all the other gamma-ray sources within 6°5 of the target galaxy in the background-only fitting, and then use the obtained indices of these sources for the subsequent analysis.

Table 1
New Sources Detected in the Survey

Name	d_L (Mpc)	Optical Center (R.A., Decl.)	Gamma-Ray Location (R.A., Decl.)	$F_{0.1-100\ \mathrm{GeV}}$ (10^{-12} erg cm^{-2} s^{-1})	Γ	TS
(1)	(2)	(3)	(4)[a]	(5)[b]	(6)	(7)
SN 2004dj	3.49	(114°321, 65°599)	(114°395, 65°573) ± 0°041[c]	2.29 ± 0.51[c]	1.92 ± 0.07[c]	73.1[c]
Arp 299	47.74	(172°136, 58°561)	(172°050, 58°526) ± 0°111	1.08 ± 0.28	2.07 ± 0.20	27.8
M33	0.84	(23°475, 30°669)	(23°609, 30°784) ± 0°089	1.28 ± 0.42	2.23 ± 0.24	25.1

Notes. (1) Source name; (2) optical R.A. J2000; (3) optical decl. J2000; (4) best location of the γ-ray source detected by Fermi-LAT; (5) 100 MeV–100 GeV γ-ray average fluxes; (6) power-law spectral photon index derived by broad band spectrum fitting; (7) TS value of the gamma-ray sources.

[a] The uncertainties of the position correspond to 95% containment radius, which are derived by fitting the distribution of LTS to a 2D Gaussian function.

[b] The fluxes and errors were computed in the 0.1–100 GeV band, from our analysis in the 0.3–500 GeV band, taking into account the covariance matrix of the maximum-likelihood fit to the data.

[c] These values are derived for the first 5.7 yr period (2008 August 4 (UT)–2014 March 25 (UT)).
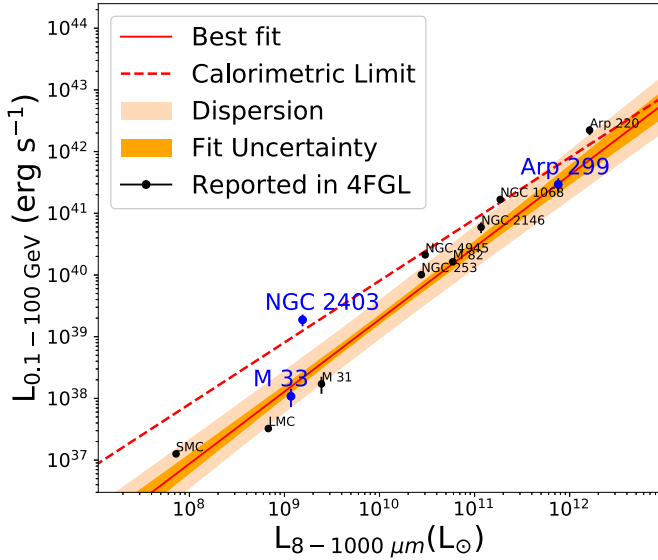

Figure 1. Gamma-ray luminosity (0.1–100 GeV) vs. total IR luminosity (8–1000 μm) for nearby star-forming galaxies. The orange band represents the empirical correlation $\log(L_{0.1-100\ \mathrm{GeV}}/\mathrm{erg\ s}^{-1}) = (1.17 \pm 0.07)$ $\log(L_{8-1000\ \mu m}/10^{10}\ L_\odot) + (39.28 \pm 0.08)$ with an intrinsic dispersion, which is taken to be normally distributed in the logarithmic space with a standard deviation of $\sigma_D = 0.24$ (Ackermann et al. 2012). The gamma-ray luminosities for the galaxies reported in 4FGL are derived from the catalog value (black points; Abdollahi et al. 2020), or based on the 11.4 yr averaged flux obtained in this work (blue points). The uncertainties on the data points are statistical only. The infrared luminosities are from Sanders et al. (2003). The calorimetric limit represents that all the energy of CR protons accelerated by supernova remnants is lost to secondary pions. We assumed a power-law spectrum of CR protons with index 2.2 and an average CR energy per SN of 10^{50} erg, similar to that given in Ackermann et al. (2012).

We use the catalogs from the NASA/IPAC Extragalactic Database (NED) and SIMBAD Database to search for possible counterparts of the gamma-ray source. Due to the nondetection of gamma-ray emission during the second half of the interval of Fermi observations, we use the data of the first 5.7 yr only to relocalize the gamma-ray emission, which is shown in Figure 3. We do not find any Galactic sources (i.e., novae, pulsars, gamma-ray binaries) or promising extragalactic gamma-ray emitters such as blazars located within the 95% error region of the gamma-ray emission. Two faint radio sources (i.e., NVSS J073724+653628 and NGC 2403:[ECB2002] alpha) with an unknown nature are located within the 95% error region. The 1.4 GHz flux densities are 4 ± 0.6 mJy for
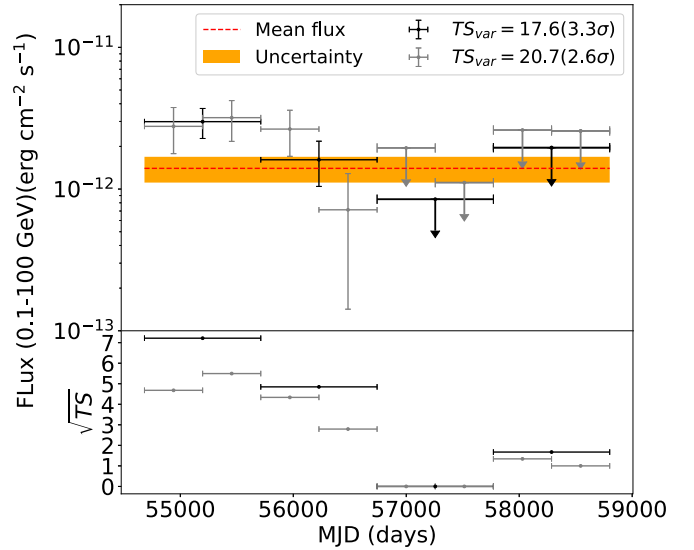

Figure 2. Light curves (upper panel) and TS values (lower panel) of the gamma-ray source 4FGL J0737.4+6535 with four and eight time bins, respectively. The mean flux is the averaged flux over the 11.4 yr analysis. The upper limits at the 95% confidence level are derived when the TS value for the data points is lower than 4. Note that the energy band in this analysis is also 300 MeV–500 GeV.

NVSS J073724+653628 (Condon et al. 1998) and ∼1.9 mJy for NGC 2403:[ECB2002] alpha (Eck et al. 2002). If the radio sources are background radio galaxies, which constitute the dominant mJy radio source population at 1.4 GHz (Norris 2017), we can estimate the gamma-ray flux assuming that the gamma-ray emission arises from inverse Compton scattering of the radio-emitting electrons off the cosmic microwave background (CMB) photons, a reasonable expectation in light of the conclusion reached by Abdo et al. (2010b). We use the simple scaling $F_C \approx F_S \rho_0/\rho_B$, where F_C is the total Compton flux, F_S is the radio flux, and $\rho_0 \simeq 4 \times 10^{-13}(1+z)^4$ erg cm^{-3} and $\rho_B = B^2/8\pi$ are the CMB energy density at redshift z and magnetic field energy density, respectively. The expected gamma-ray fluxes of the two radio sources (assuming $z = 1$) are only at the level of ∼10^{-14} erg cm^{-2} s^{-1} for $B \sim 1\ \mu$G, which is about two orders of magnitude lower than the observed flux. The expected gamma-ray flux would be more consistent with the measured one if these two radio sources are blazars. However, the latter source has a mid-infrared colors (Cutri et al. 2013) not compatible with those of blazars
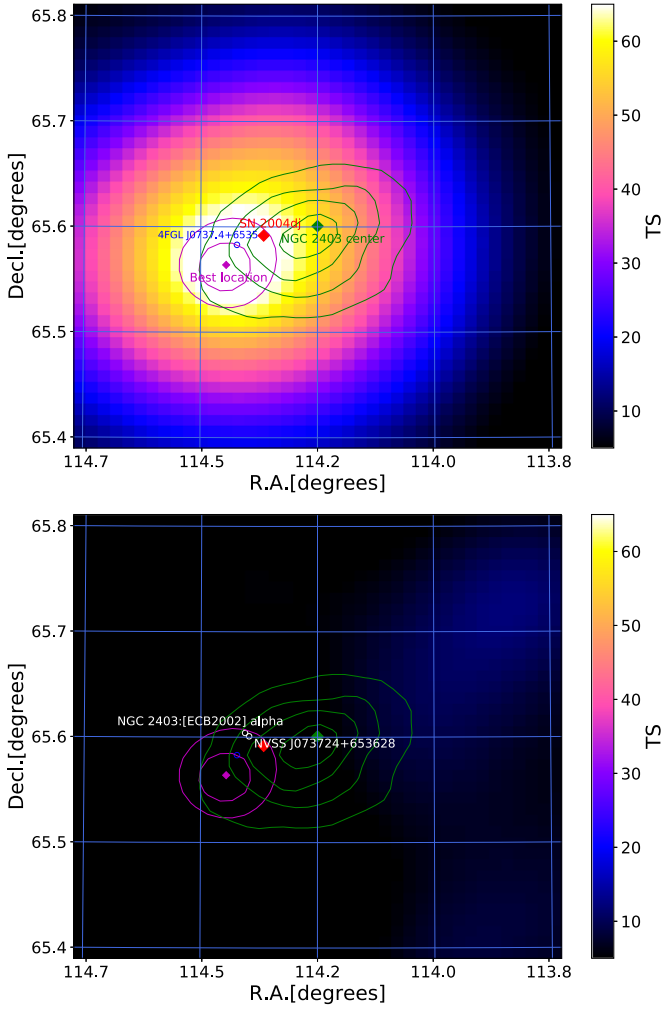
Figure 3. TS map in the energy band 0.3–500 GeV for the first 5.7 yr analysis (top) and for the second 5.7 yr analysis (bottom). The purple contours represent the 68% and 95% C.L. region of the gamma-ray source. The dark green contours represent the IR map of NGC 2403 measured by IRAS at 60 μm.

(D'Abrusco et al. 2014). It also has an X-ray counterpart (Binder et al. 2015) with a flux of $\sim 3 \times 10^{-16}$ erg cm^{-2} s^{-1} in 0.35–8 keV, which suggests that it might be an X-ray binary in NGC 2403 with an X-ray luminosity $\sim 4 \times 10^{35}$ erg s^{-1}. The measured gamma-ray luminosity $\sim 10^{39}$ erg s^{-1} would then be too high to come from this X-ray source, since the GeV luminosities of X-ray binaries detected in our Galaxy are $\lesssim 10^{36}$ erg s^{-1} (Dubus 2013). We cannot rule out completely the possibility of the former source being a blazar. However, the probability is quite small because the amount of blazars satisfying the measured gamma-ray spectral feature is small.[8]

---

[8] The maximum photon energy detected by LAT is 267.1 GeV, and there is no hint of a softening or cutoff feature in the gamma-ray spectrum. This limits the distance of the gamma-ray source to be $z < 0.3$ so that the opacity of the extragalactic background light (EBL) absorption (Finke et al. 2010) will not exceed unity. Following the gamma-ray luminosity function of the luminosity-dependent density evolution (LDDE) model suggested by Ajello et al. (2014), the total number of blazars including BL Lac objects and flat-spectrum radio quasars is ~ 60 for those located at $z < 0.3$ and to be consistent with the observed gamma-ray flux ($L_\gamma/4\pi D_L(z)^2 \in [1.78, 2.80] \times 10^{-12}$ erg cm^{-2}s^{-1}) and the spectral index ($\Gamma \in [1.85, 1.99]$) at the 1σ level. On the other hand, the number of radio sources with 1.4 GHz flux $\in [3.4, 4.6]$ mJy is $\sim 25,000$. Therefore the probability of the radio source being a blazar is $\sim 60/25,000 = 0.0024$, which can be rejected at the 3σ level.

Therefore, it is unlikely that the gamma-ray emission comes from the two radio sources.

On the other hand, we find a recent supernova explosion, SN 2004dj, occurred in the error region of the gamma-ray source. SN 2004dj is peculiar in that it is the second nearest supernova to Earth (after SN 1987A). The probability of chance coincidence between the gamma-ray source and SN 2004dj is estimated to be 0.0022 (see Appendix A for more details). Combining with the transient nature of the gamma-ray source, we suggest that it is physically associated with SN 2004dj.

4. Discussion and Conclusion

The GeV emission may originate from the dissipation of the kinetic energy of the SN ejecta, either internally (which may be analogous to the case of a nova; e.g., Li et al. 2017) or externally. In the latter scenario, which is more common for a supernova, the ejecta may encounter a dense gas shell (or clump) in the vicinity of the SN progenitor and drive a strong shock. The gas shell may be formed by the stellar wind of the progenitor star (Dwek 1985). It is not clear at which epoch the shock is driven, but apparently it could be as early as a time period shortly after the SN explosion, so we assume that the shock has been launched somewhere around the beginning of the Fermi mission, i.e., at $t_{\mathrm{LAT},0} = 1465.6$ days (approximately 4 yr), with respect to the SN explosion. Assuming a mass of $M_{\mathrm{ej}} = 10 \, M_\odot$ for the ejecta and a total kinetic energy of $E_k = 10^{51}$ erg, the bulk of the ejecta moves with a velocity of $v_{\mathrm{ej}} = \sqrt{2E_k/M_{\mathrm{ej}}} = 3000$ km s^{-1} and leads to a shock radius of at least $R_{\mathrm{sh}} = v_{\mathrm{ej}} t_{\mathrm{LAT},0} \simeq 4 \times 10^{16}$ cm. The distance of the interior shell to the SN progenitor is not supposed to be larger than R_{sh}. Considering that generally $\lesssim 10\%$ of the dissipated kinetic energy of the SN ejecta could be converted to nonthermal particles (Aharonian et al. 2004), the energy in nonthermal particles can reach as high as $\sim 10^{50}$ erg. Given that the total gamma-ray energy detected by Fermi-LAT is $\sim 6 \times 10^{47}$ erg,[9] we find that $\gtrsim 0.6\%$ of the ejecta's kinetic energy is needed to be dissipated. As the shock energy is proportional to the ratio between the swept-up material mass and the SN ejecta mass, this implies that a total amount of material of $\geqslant 0.06 \, M_\odot$ is swept up by the shock. As the shock sweeps through the shell, it accelerates protons and electrons therein to relativistic energies. In principle, both electrons and protons can radiate gamma-rays, through inverse Compton (IC) scatterings off ambient photons or the decay of π^0 produced in pp collisions, respectively.

In the leptonic scenario, the target photon field for the IC radiation of electrons is a ~ 500 K thermal radiation with a total luminosity of $L_{\mathrm{IR}} \sim 4 \times 10^{38}$ erg s^{-1} from the dust formed in the SN ejecta (Meikle et al. 2011; Szalai et al. 2011; Fox et al. 2013), inferred from the observation of Spitzer overlapping with the first one and a half year of Fermi-LAT's observation (i.e., until 2010 May 23). The photon energy density at the shock downstream is given by $u_{\mathrm{IR}} \simeq 10^{-7}(R_{\mathrm{sh}}/10^{17}\,\mathrm{cm})^{-2}$ erg cm^{-3}, yielding an IC cooling timescale of $t_{\mathrm{IC}} \simeq 100(E_e/50\mathrm{GeV})^{-1}(R_{\mathrm{sh}}/10^{17}\,\mathrm{cm})^2$ yr. In the meantime, the accelerated electrons will also radiate in the downstream magnetic field of the shock via the synchrotron process. The ratio between the IC emissivity and the synchrotron

---

[9] The total energy in the 0.1–100 GeV energy band is $E_\gamma = 4\pi D_L^2 F_\gamma \delta T \simeq 6 \times 10^{47}$ erg, where $F_\gamma = 2.29 \times 10^{-12}$ erg cm^{-2} s^{-1}, $\Delta T = 5.7$ yr, and $D_L = 3.5$ Mpc.
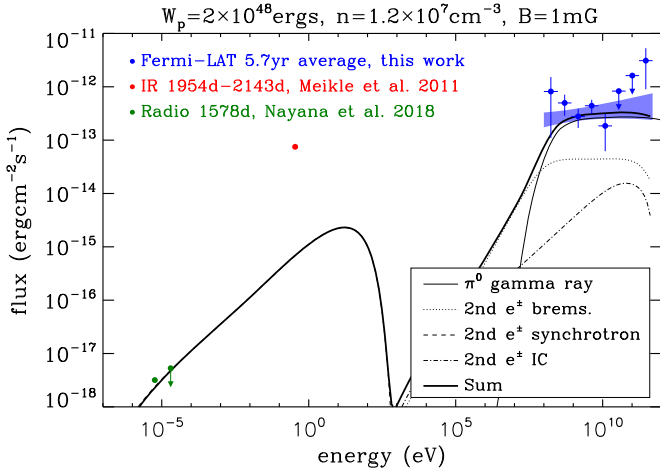
Figure 4. Multiwavelength spectrum of SN 2004dj and the theoretical expectation in the hadronic interpretation. The blue points are the first 5.7 yr averaged flux obtained in this work. The upper limits at 95% C.L. are derived when the TS value for the data points are lower than 4. The blue shaded region marks the 1σ uncertainty for a power-law fitting to the data. The red point represents Spitzer's observation (after subtracting the contribution of the host galaxy; Meikle et al. 2011), and the green points represent the radio fluxes measured by VLA (Nayana et al. 2018). The thin solid curve shows pionic gamma-ray flux from pp collisions. The dotted, dashed, and dashed–dotted curves are the flux from the bremsstrahlung, synchrotron, and inverse Compton processes emitted by the secondary $e^{\pm}$ pairs produced in pp collisions. Model parameters are shown in the top of the panel. See Section 4 for more discussion.

emissivity of an electron is equal to the ratio between the energy density of the target photon field and that of the magnetic field. On the other hand, the synchrotron radiation flux should not be larger than 0.227 mJy at 1.4 GHz as observed by the Very Large Array (VLA) after 1578 days of the explosion (Nayana et al. 2018). Therefore, as the gamma-ray flux is ascribed to the IC radiation of accelerated electrons, it constrains the downstream magnetic field to be $B < 12 \ (R_{sh}/10^{17}\,{\rm cm})^{-4/3}\,\mu{\rm G}$ (see Appendix B for details). Given that $R_{sh} \simeq 4 \times 10^{16}$ cm at the operation starting time of Fermi-LAT, we obtain a more conservative upper limit for the downstream magnetic field $B < 41 \ \mu{\rm G}$, noting that it is supposed to decrease with time. This value is probably too low considering that the inferred magnetic fields of some well-studied SNRs, such as Cassiopeia A, Tycho, Kepler, SN 1006, and G347.3-0.5, at a much later evolution stage (i.e., from several hundred to several thousand years after the SN explosion) is $\gtrsim 0.1$ mG (Reynolds et al. 2012, and reference therein), and therefore the leptonic interpretation is not favored.

On the other hand, the energy-loss timescale of a proton via the pp collision is $t_{pp} = 7 \times 10^7 (n/1\,{\rm cm}^{-3})^{-1}$ yr, where n is the target gas density. About one-third of the lost energies will go into pionic gamma-rays. We calculate the pionic gamma-ray spectrum and the secondary electron/positron pair spectrum from the pp collision with the parameterized formulae given by Kamae et al. (2006). The result is shown in Figure 4. The total energy of the accelerated protons is assumed to be $W_p = 2 \times 10^{48}$ erg with a differential spectrum in a power-law distribution with slope -2 in the range of 1 GeV–1 TeV. The atom density of the gas shell is set to be $n = 1.2 \times 10^7$ cm^{-3}, so that protons will cool in 5.7 yr. With this

assumption, the nondetection of gamma-ray emission in the second 5.7 yr (2014 March 25 (UT)–2019 November 14 (UT)) could be explained as that the proton acceleration has stopped provided the shell's thickness $\Delta < v_{ej} \times 5.7$ yr $= 5.4 \times 10^{16}$ cm, while protons accelerated earlier have already depleted their energies in pp collisions. Assuming that the shell is located at $R = 4 \times 10^{16}$ cm and that the shell's thickness is 0.1 of the radius, the total mass of the shell is found to be $0.8 M_{\odot}$ with the proposed density. This is consistent with the mass loss of a star in the red supergiant phase of its evolution (Smith et al. 2009; Beasor & Davies 2018). In order to suppress the synchrotron radiation of the secondary pairs to the level consistent with the VLA measurement, we find the downstream magnetic field needs to be weaker than 1 mG.

To summarize, using 11.4 yr of Fermi-LAT observations, we searched for possible gamma-ray emission from nearby galaxies in the IRAS Revised Bright Galaxies Sample. In additional to the new detection of gamma-ray emission from two nearby galaxies, Arp 299 and M33, we find a gamma-ray source in the region of the galaxy NGC 2403. The gamma-ray source cannot be explained as pionic gamma-ray emission from the CR–ISM interaction in NGC 2403, as it appears as an outlier of the $L_{0.1-100\,{\rm GeV}} - L_{8-1000\,\mu m}$ correlation for star-forming galaxies and has a fading flux with time. On the other hand, we find that SN 2004dj, the second nearest supernova, is spatially and temporally consistent with the fading gamma-ray source. The probability of the chance coincidence of SN 2004dj with an unrelated background gamma-ray source is estimated to only 0.0022 based on the 4FGL catalog. We interpret this gamma-ray emission arising from the supernova ejecta interacting with a surrounding high-density shell, which converts ~1% of the ejecta's kinetic energy to relativistic protons. This shows that supernovae can accelerate cosmic-ray protons at a very early stage of their lives.

Appendix A
Estimate the Chance Coincidence

Using a Poisson distribution, the chance probability of observing a background source in the position of SN 2004dj is $P_{ch} = 1 - \exp[-\pi(R_0^2 + 4\sigma_\gamma^2)\sum(>F_{th})]$, where $\sum(>F_{th})$ is the surface density of Fermi-LAT sources with fluxes higher than F_{th}, σ_γ is the 68% position uncertainties of Fermi-LAT counterpart, and R_0 is the angular distance between the gamma-ray location and the target source SN 2004dj. Since the density distribution of the 4FGL sources in the box defined by $|\sin(b)| > 0.25$ is uniform with respect to the angle, we estimate a number density of $\sum(>F_{th}) = 579.4\,{\rm sr}^{-1}$ above the flux $F_{th} = 1.18 \times 10^{-12}\,{\rm erg\,cm}^{-2}\,{\rm s}^{-1}$, using the power-law fitting of the cumulative numbers of sources as a function of the threshold fluxes for the 4FGL sources, as shown in Figure A1. Then the chance coincidence probability is estimated to be 0.0022 for $R_0 = 0°\!.041$ and $\sigma_\gamma = 0°\!.024$.
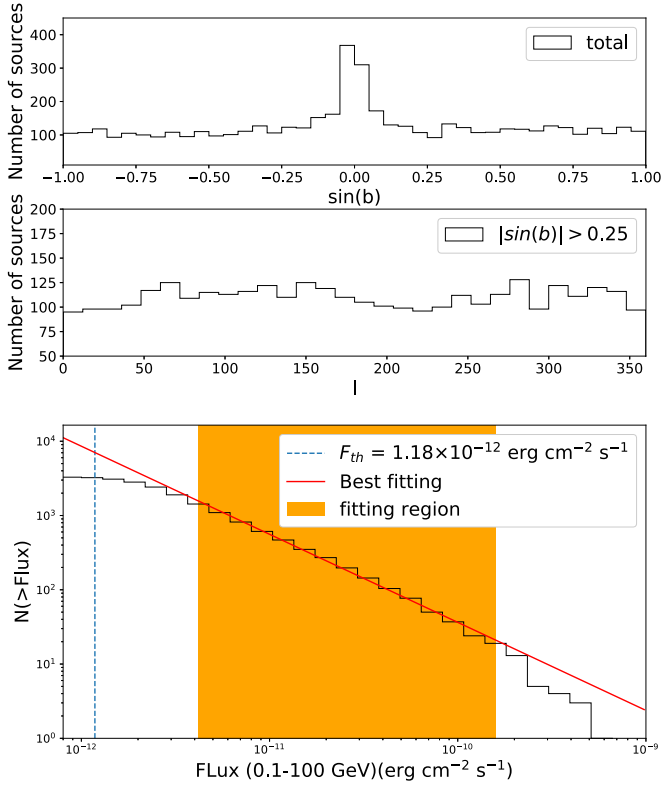
Figure A1. Upper panel: 4FGL source number distribution in Galactic latitude b. Middle panel: 4FGL source number distribution in Galactic longitude for $|\sin(b)| > 0.25$. Lower panel: cumulative source count distribution of 4FGL sources with $|\sin(b)| > 0.25$. The Fermi-LAT point source sensitivity ($F_{\rm th}$) at the position of SN 2004dj can be given by $F_{\rm th} = F_{\rm U.L.}\left(\frac{5.7\,{\rm yr}}{8\,{\rm yr}}\right)^{\frac{1}{2}}$, where $F_{\rm U.L.} = 1.39 \times 10^{-12}\,{\rm erg\,cm^{-2}\,s^{-1}}$ is the 95% upper limit obtained from the second 5.7 yr analysis.

Appendix B
Derivation of the Magnetic Field Upper Limit

Leptonic scenario. The average gamma-ray luminosity in 0.1–100 GeV is $L_{\gamma,\,0.1–100\,{\rm GeV}} = 3.3 \times 10^{39}\,{\rm erg\,s^{-1}}$. Approximating the photon index to be -2, the differential luminosity (i.e., $E_\gamma^2 dN/dE_\gamma dt$) is $L_\gamma(E_\gamma) = L_{\gamma,0.1–100\,{\rm GeV}}/\log(1000) = 4.8 \times 10^{38}\,{\rm erg\,s^{-1}}$, independent of the photon energy. As we ascribe the gamma-ray emission to the IC radiation of accelerated electrons, $L_\gamma(E_\gamma)$ should be equal to the total power of electrons at energy E_e, where

$$E_e = 50(T_{\rm IR}/500\,{\rm K})^{-1/2}(E_\gamma/1\,{\rm GeV})^{1/2}\,{\rm GeV}. \quad (B1)$$

The differential energy spectrum of electrons can be found by $E_e^2 dN/dE_e = L_\gamma(E_\gamma)t_{\rm IC}(E_e) = 1.5 \times 10^{48}(E_e/50\,{\rm GeV})^{-1}(R_{\rm sh}/10^{17}\,{\rm cm})^2$ erg. According to Equation (B1), we find the energy of electrons responsible for 0.1 GeV gamma-rays to be 16 GeV. To calculate the synchrotron luminosity in the radio band, we need to extrapolate the electron spectrum to energies below 16 GeV. Note that to explain the photon index of -2, the electron spectral index above 16 GeV needs to be -3. We assume a break at 16 GeV and a flat spectrum ($dN/dE_e \propto E_e^{-2}$) below 16 GeV to reduce the predicted radio flux. Such a flat spectrum is also consistent with the prediction of the canonical diffusive shock acceleration theory for strong shocks (Bell 1978). As such, we have

$$E_e^2 dN/dE_e = 4.7 \times 10^{48}(R_{\rm sh}/10^{17}\,{\rm cm})^2 \quad {\rm for} \quad E_e < 16\,{\rm GeV}.$$

The synchrotron cooling timescale of electrons radiating at a characteristic frequency ν is

$$t_{\rm syn} = 4.2 \times 10^7 \left(\frac{\nu}{1.4\,{\rm GHz}}\right)^{-1/2} B^{-3/2}\,{\rm s}. \quad (B2)$$

Then we can estimate the synchrotron luminosity by

$$L_{\rm syn}(\nu) = \frac{E_e^2 dN/dE_e}{t_{\rm syn}}$$

$$= 1.1 \times 10^{41} \left(\frac{R_{\rm sh}}{10^{17}\,{\rm cm}}\right)^2 \left(\frac{\nu}{1.4\,{\rm GHz}}\right)^{1/2} B^{3/2}\,{\rm erg\,s^{-1}}. \quad (B3)$$

The 1.4 GHz luminosity observed by VLA is $4.6 \times 10^{33}\,{\rm erg\,s^{-1}}$ at 1578 days after the explosion (Nayana et al. 2018). Since there could be other processes contributing to the flux, $L_{\rm syn}$ should be smaller than this value, and this results in $B < 12(R_{\rm sh}/10^{17}\,{\rm cm})^{-4/3}\,\mu{\rm G}$. Such a strong limit on the magnetic field might in principle be relaxed, if one argues the possible existence of an extra intense radiation field around the SN during the period of Fermi-LAT's detection, which in the meantime is hidden to observers, or if one argues a low-energy cutoff present in the electron spectrum above the energy responsible for radio emission. These two possibilities are, however, not supported either observationally or theoretically, so we do not discuss them further in this work.

Hadronic scenario. In pp collisions, approximately one-third of produced pions are neutral pions and the other two-thirds are charged pions that will decay into neutrinos and electrons/positrons (hereafter we do not distinguish positrons from electrons for simplicity) with a ratio of 3:1. On average, the energy of a secondary electron is half of the energy of a gamma-ray photon produced by protons of the same energy, while the secondary electron energy production rate is also half of that of gamma-rays, i.e.,

$$E_e^2 \frac{dN_{\rm 2nd}}{dE_e dt} = \frac{1}{2}L_\gamma(E_\gamma) = 2.4 \times 10^{38}\,{\rm erg\,s^{-1}}, \quad (B4)$$

for $50\,{\rm MeV} < E_e < 50\,{\rm GeV}$. The radio-emitting electrons cannot be cooled during Fermi-LAT's detection period, so the accumulated secondary electron spectrum can be given by $E_e^2(dN_{\rm 2nd}/dE_e) = E_e^2(dN_{\rm 2nd}/dE_e dt)\tau_{\rm GeV}$, with $\tau_{\rm GeV}$ being the duration of the GeV emission. The duration should last at least 5.7 yr as Fermi-LAT detected, while it can be at longest 9.7 yr if the GeV emission starts shortly after the SN explosion. Similar to Equation (B3), we estimate the synchrotron luminosity of secondary electrons by

$$L_{\rm syn,2nd}(\nu) = \frac{E_e^2 dN_{\rm 2nd}/dE_e}{t_{\rm syn}}$$

$$= 1.7 \times 10^{39} \left(\frac{\tau_{\rm GeV}}{9.7\,{\rm yr}}\right) \left(\frac{\nu}{1.4\,{\rm GHz}}\right)^{1/2} B^{3/2}\,{\rm erg\,s^{-1}}, \quad (B5)$$

and we get $B < 1.9(\tau_{\rm GeV}/9.7\,{\rm yr})^{-2/3}\,{\rm mG}$ by requiring Equation (B5) be smaller than the measured 1.4 GHz luminosity $4.6 \times 10^{33}\,{\rm erg\,s^{-1}}$. This result is consistent with

the one obtained in Section 4 (see also Figure 4) by a more accurate numerical calculation.

ORCID iDs

Ruo-Yu Liu ![ORCID] https://orcid.org/0000-0003-1576-0961
Xiang-Yu Wang ![ORCID] https://orcid.org/0000-0002-5881-335X
Bing Zhang ![ORCID] https://orcid.org/0000-0002-9725-2524

References

Abdo, A. A., Ackermann, M., Ajello, M., et al. 2010a, ApJL, 709, L152
Abdo, A. A., Ackermann, M., Ajello, M., et al. 2010b, Sci, 328, 725
Abdollahi, S., Acero, F., Ackermann, M., et al. 2020, ApJS, 247, 33
Acero, F., Ackermann, M., Ajello, M., et al. 2016, ApJS, 223, 26
Ackermann, M., Ajello, M., Allafort, A., et al. 2012, ApJ, 755, 164
Ackermann, M., Arcavi, I., Baldini, L., et al. 2015, ApJ, 807, 169
Aharonian, F. A., Akhperjanian, A. G., Aye, K.-M., et al. 2004, Natur, 432, 75
Ajello, M., Romani, R. W., Gasparrini, D., et al. 2014, ApJ, 780, 73
Atwood, W. B., Abdo, A. A., Ackermann, M., et al. 2009, ApJ, 697, 1071
Beasor, E. R., & Davies, B. 2018, MNRAS, 475, 55
Bell, A. R. 1978, MNRAS, 182, 147
Berezhko, E. G., Ksenofontov, L. T., & Völk, H. J. 2011, ApJ, 732, 58
Berezhko, E. G., Ksenofontov, L. T., & Völk, H. J. 2015, ApJ, 810, 63
Binder, B., Williams, B. F., Eracleous, M., et al. 2015, AJ, 150, 94
Chakraborti, S., Yadav, N., Ray, A., et al. 2012, ApJ, 761, 100
Condon, J. J., Cotton, W. D., Greisen, E. W., et al. 1998, AJ, 115, 1693
Cutri, R. M., Wright, E. L., Conrow, T., et al. 2013, Explanatory Supplement to the AllWISE Data Release Products, http://wise2.ipac.caltech.edu/docs/release/allwise/expsup/index.html
D'Abrusco, R., Massaro, F., Paggi, A., et al. 2014, ApJS, 215, 14
Dubus, G. 2013, A&ARv, 21, 64
Dwek, E. 1985, ApJ, 297, 719
Eck, C. R., Cowan, J. J., & Branch, D. 2002, ApJ, 573, 306
Finke, J. D., Razzaque, S., & Dermer, C. D. 2010, ApJ, 712, 238
Fox, O. D., Filippenko, A. V., Skrutskie, M. F., et al. 2013, AJ, 146, 2
Griffin, R. D., Dai, X., & Thompson, T. A. 2016, ApJL, 823, L17
Kamae, T., Karlsson, N., Mizuno, T., Abe, T., & Koi, T. 2006, ApJ, 647, 692
Li, K.-L., Metzger, B. D., Chomiuk, L., et al. 2017, NatAs, 1, 697
Li, Z. 2019, SCPMA, 62, 959511
Malyshev, D., Pühlhofer, G., Santangelo, A., & Vink, J. 2019, arXiv:1903.03045
Meikle, W. P. S., Kotak, R., Farrah, D., et al. 2011, ApJ, 732, 109
Murase, K., Thompson, T. A., Lacki, B. C., et al. 2011, PhRvD, 84, 043003
Nakano, S., Itagaki, K., Bouma, R. J., Lehky, M., & Hornoch, K. 2004, IAUC, 8377, 1
Nayana, A. J., Chandra, P., & Ray, A. K. 2018, ApJ, 863, 163
Nolan, P. L., Abdo, A. A., Ackermann, M., et al. 2012, ApJS, 199, 31
Norris, R. P. 2017, NatAs, 1, 671
Patat, F., Benetti, S., Pastorello, A., Filippenko, A. V., & Aceituno, J. 2004, IAUC, 8378, 1
Peng, F.-K., Wang, X.-Y., Liu, R.-Y., Tang, Q.-W., & Wang, J.-F. 2016, ApJL, 821, L20
Peng, F.-K., Zhang, H.-M., Wang, X.-Y., Wang, J.-F., & Zhi, Q.-J. 2019, ApJ, 884, 91
Renault-Tinacci, N., Kotera, K., Neronov, A., et al. 2018, A&A, 611, A45
Reynolds, S. P., Gaensler, B. M., & Bocchino, F. 2012, SSRv, 166, 231
Sanders, D. B., Mazzarella, J. M., Kim, D. C., Surace, J. A., & Soifer, B. T. 2003, AJ, 126, 1607
Smith, N., Hinkle, K. H., & Ryde, N. 2009, AJ, 137, 3558
Szalai, T., Vinkó, J., Balog, Z., et al. 2011, A&A, 527, A61
Tang, Q.-W., Wang, X.-Y., & Tam, P.-H. T. 2014, ApJ, 794, 26
Vinkó, J., Takáts, K., Sárneczky, K., et al. 2006, MNRAS, 369, 1780
Wang, K., Huang, T.-Q., & Li, Z. 2019, ApJ, 872, 157
Xi, S.-Q., Zhang, H.-M., Liu, R.-Y., et al. 2020, arXiv:2003.07830
Yuan, Q., Liao, N.-H., Xin, Y.-L., et al. 2018, ApJL, 854, L18
Zhang, Y., Peng, F.-K., & Wang, X.-Y. 2019, ApJ, 874, 173